The Role of Schlemm's Canal Endothelium Cellular Connectivity in Giant Vacuole Formation: A 3D Electron Microscopy Study

Julia Lai,[1] Yanfeng Su,[1,2] David L. Swain,[1,3] Davy Huang,[1] Dimitr Getchevski,[1] and Haiyan Gong[1,3]

[1]Department of Ophthalmology, Boston University School of Medicine, Boston, Massachusetts, United States
[2]The Affiliated Eye Hospital of Wenzhou Medical University, Wenzhou, Zhejiang, China
[3]Department of Anatomy and Neurobiology, Boston University School of Medicine, Boston, Massachusetts, United States

Correspondence: Haiyan Gong, Department of Ophthalmology, Boston University School of Medicine, 72 East Concord Street, Room L-905, Boston, MA 02118, USA; hgong@bu.edu.

Submitted: October 18, 2018
Accepted: March 14, 2019

Citation: Lai J, Su Y, Swain DL, Huang D, Getchevski D, Gong H. The role of Schlemm's canal endothelium cellular connectivity in giant vacuole formation: a 3D electron microscopy study. *Invest Ophthalmol Vis Sci*. 2019;60:1630–1643. https://doi.org/10.1167/iovs.18-26011

Purpose. We investigated whether cellular connectivity between Schlemm's canal (SC) inner wall (IW) endothelium, and juxtacanalicular connective tissue (JCT), and between IW endothelial cells, plays a role in giant vacuole (GV) and pore formation by comparing perfusion- and immersion-fixed eyes.

Methods. Normal human donor eyes ($n = 4$) were either immersion-fixed (0 mm Hg) or perfusion-fixed (15 mm Hg). Trabecular meshwork near SC was imaged using serial block-face scanning electron microscopy. A total of 12 IW cells from each group were 3D-reconstructed from ~7040 electron micrographs and compared. In each cell, connections between IW cells and JCT cells/matrix were quantified; IW/IW connectivity was measured by cell border overlap length. GV volume, density, shape, and intracellular and paracellular pores were analyzed.

Results. The mean number of IW/JCT cell-cell connections per cell significantly decreased ($P < 0.01$) while the summed GV volume per cell significantly increased ($P < 0.01$) in perfusion-fixed eyes compared to immersion-fixed eyes. Intracellular pores were observed in 14.6% of GVs in perfusion-fixed eyes and not observed in immersion-fixed eyes. The mean IW/IW overlap length per cell decreased ($P < 0.01$), and paracellular pores were found only in regions where IW/IW connectivity was minimal (overlap length = 0 μm) in perfusion-fixed eyes and not observed in immersion-fixed eyes.

Conclusions. Our data suggest that changes in IW/JCT connectivity may be an important factor in the formation of larger GVs, and decreased IW/IW connectivity may promote paracellular pore formation. Targeting the IW/JCT and IW/IW connectivity may therefore be a potential strategy to regulate outflow resistance and IOP.

Keywords: Schlemm's canal endothelium, cellular connectivity, giant vacuoles, pores, serial block-face scanning electron microscopy, 3D electron microscopy

Primary open-angle glaucoma (POAG) is a leading cause of blindness worldwide.[1] A primary risk factor for POAG is elevated intraocular pressure (IOP) from increased aqueous outflow resistance.[2–4] Most of the resistance is believed to be generated in the juxtacanalicular connective tissue (JCT) and modulated by the inner wall (IW) of Schlemm's canal (SC).[5–11] However, the mechanism through which outflow resistance is regulated remains unclear.

Rho-kinase inhibitors have been shown to increase outflow facility and to be associated with a physical separation between the IW and the underlying JCT in porcine,[12] bovine,[13] and monkey eyes[14] and with JCT expansion in human eyes.[15–17] JCT expansion and separation from the IW have also been observed in increasing outflow facility during washout in bovine eyes.[14,18] These studies suggest that IW/JCT connectivity may play a role in regulating outflow resistance. Furthermore, passage of aqueous humor into SC appears to require formation of giant vacuoles (GVs) and pores, and previous studies showed an increased pore density with increased accumulation of fluorescent tracers along the IW[19] and near the pores on both basal and apical sides of the IW endothelium of SC.[15] In previous studies of POAG eyes, there was an observed overall reduction in pore density compared to age-matched normal eyes.[10,20] Previous electron microscopy studies have investigated GV size with different perfusion pressures and described types of connections between IW and JCT cells in 1000 regions of contact between cells using random sections.[21] However, due to lack of methods, no previous study has been able to quantify accurately the degree of IW/JCT connectivity and GV volume in each individual IW cell. Therefore, the relationships between IW/JCT connectivity and GV and intracellular pore (I-pore) formation have not been fully elucidated. Additionally, a previous study reported that with increasing IOP, tight junctions connecting adjacent IW cells became simplified, and the overlap between IW cells decreased.[22] However, the relationship between decreased IW/IW connectivity and paracellular or border pore (B-pore)

Table 1. Five Tissue Blocks Dissected From Four Donor Eyes Were Processed for Serial Block-Face Scanning Electron Microscopy

Tissue Block	Donor	Fixation Condition	Number of Images Per Block	Field Size, μm^2	Resolution, nm/Pixel	Thickness, µm	IW Cells Reconstructed
(A)	Eye 01	Immersion-fixed	810	141.56 × 60.67	10.1	0.13	3
(B)	Eye 02	Immersion-fixed	1091	103.40 × 51.70	10.1	0.15	9
(C)	Eye 03	Perfusion-fixed	2181	141.49 × 62.86	10.1	0.13	3
(D)	Eye 04	Perfusion-fixed	1380	141.73 × 60.51	10.1	0.13	4
(E)	Eye 04	Perfusion-fixed	1578	141.57 × 60.67	10.1	0.13	5

formation has not yet been studied also due to lack of an effective method.

Serial block-face scanning electron microscopy (SBF-SEM), in combination with 3D-reconstruction, was first introduced for examining large volumes of neuronal tissue.[23] In neuroscience, this technique allows researchers to study synaptic interactions of neurons in 3D through a substantial spatial volume of neuronal circuits.[23–27] In ophthalmology research, it was used to study the 3D aspects of matrix assembly by cells in the developing cornea[28] and to gain a structural understanding of retinal degeneration.[29] In this study, using this innovative method and large serial image sets, we investigated whether cellular connectivity between IW endothelial cells of SC and JCT cells/matrix and between adjacent IW cells plays a role in GV and pore formation by comparing 3D reconstructed IW cells from perfusion-fixed (15 mm Hg) eyes to immersion-fixed (0 mm Hg) eyes.

The goal of this study was to test our hypothesis that larger GVs in perfusion-fixed eyes are associated with a decrease in IW/JCT connectivity and increased I-pore formation and that a decrease in IW/IW connectivity may promote B-pore formation, and thus may contribute to the regulation of aqueous outflow resistance.

Methods

Human Donor Eyes

Four normal human donor eyes from four individual donors without any known history of ocular disease or surgery were received from National Disease Research Interchange (Eyes 01 and 02, ages = 69, 76; Philadelphia, PA, USA) and the Miracles in Sight Eye Bank (Eyes 03 and 04, ages = 74, 32; Winston-Salem, NC, USA) within 24-hours postmortem (Table 1). All eyes were confirmed to be grossly normal under dissecting microscope and were used in accordance with the guidelines regarding use of human subjects and tissue as outlined in the tenets of the Declaration of Helsinki.

Tissue Fixation

For immersion-fixation of eyes 01 and 02, a small cut (~5 mm) was made along the equator of the eyes, followed by immediate immersion in modified Karnovsky's fixative (2.5% glutaraldehyde and 2% paraformaldehyde in a 0.1-M sodium phosphate-buffer, pH = 7.3) for 24 hours.

The perfusion procedure has previously been described in detail.[30] Briefly, eyes 03 and 04 were perfused with Dulbecco's phosphate-buffered saline (pH = 7.3; GIBCO, Carlsbad, CA, USA) containing 5.5 mM D-glucose (collectively referred to as GPBS) at 15 mm Hg to establish a stable baseline facility for 30 minutes. The eyes were then perfusion-fixed at 15 mm Hg for 30 minutes with the same fixative as immersion-fixation described above. Upon completion of perfusion, a small cut (~5 mm) cut was gently made along the equator, and the eyes were immersed in the same fixative overnight.

After fixation, a total of five tissue wedges ($2 \times 2 \times 2$ mm^3) of the regions of interests (ROIs), including trabecular meshwork, SC, and small portions of sclera, were dissected from the four eyes and delivered to Renovo Neural, Inc. (Cleveland, OH, USA) for imaging by SBF-SEM.

SBF-SEM Imaging

An SBF-SEM specialist at Renovo Neural, Inc. processed and embedded the tissue wedges using a previously described technique.[31] Tissues were extensively stained with heavy metals, including osmium-ferrocyanide solution (2% osmium tetroxide), tetracarbohydrazide, uranyl acetate, and lead aspartate, and embedded in Epon resin. The ROIs in each tissue block were evaluated and confirmed by HG and subsequently imaged using a Zeiss Sigma VP SBF-SEM equipped with a serial block-face scanning electron microscopy (Gatan 3View; Gatan, Inc., Pleasanton, CA, USA) in-chamber ultramicrotome stage, with low-kV backscattered electron detectors optimized for serial block-face scanning electron microscopy systems (Gatan, Inc.). Imaging conditions are provided in Table 1. Resulting images were compiled and shipped to Boston University School of Medicine for 3D reconstruction and analyses.

3D Reconstruction

A total of 24 IW cells (n = 12 cells from each fixation condition) that were fully captured within the imaging field were randomly selected to be reconstructed. All of the images associated with these full cells were examined by trained observers (JL, YS, DLS, DG) to manually outline the cell body, cellular connections, GVs, and pores, with each cell spanning between 400 to 800 images. Out-of-field cells were not reconstructed. Outlining (tracing) of structures was performed using Reconstruct (Fiala, 2005). 3D geometries were reconstructed based on 2D outlines (traces) using Reconstruct and Amira (Thermo Fisher Scientific; for detailed methods, see Supplementary Video S1).

All measurements were taken twice by two independent observers (JL, YS, DLS, DG) to confirm the repeatability of the methods. The percentage differences for all of the measurements between any two observers were less than 10%.

Morphometric Analyses

IW Cell Dimensions. In Reconstruct, cell length of each 3D reconstructed cell was measured along the major axis (z dimension) using the Z-trace function (Fig. 1A). In ImageJ (http://imagej.nih.gov/ij/; provided in the public domain by the National Institutes of Health, Bethesda, MD, USA), cell width was measured on the SBF-SEM image where the cell showed the largest cross-sectional area of cell nucleus (Figs. 1B, 1C). The nonnuclear width was also measured on SBF-SEM images at multiple locations (at least 5) along the length of the cell (every 40 sections), and the average of those measure-

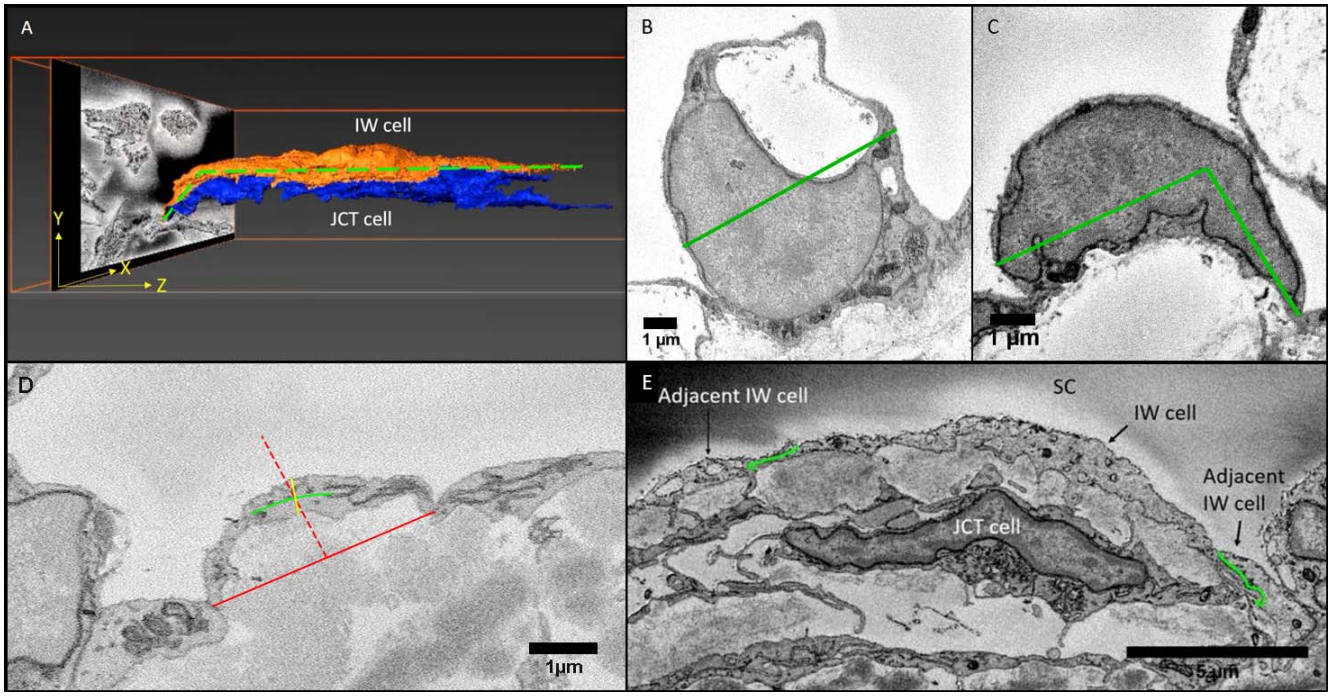

Figure 1. Methods for measurements in Reconstruct and ImageJ. (**A**) A schematic of measurement of IW cell length in 3D scene of Reconstruct software. The cell length (*green dotted line)* of the IW endothelial cell of SC was measured along its major axis in the Z-dimension using the "Z-trace" tool to autocalculate the cell length. (**B**, **C**) Cell width in nuclear area: The cell width was measured on the section where its nucleus was largest in size. When the base of the cell was flat, cell width was defined as the maximum possible width across the cell body (*green straight line*) that parallels the base of the inner wall endothelium (**B**). When the cell curved, a maximum of three marks were made along the cell axis to connect the borders of the cell (*green line*), accounting for the cell's curvature (**C**). (**D**) Cell thickness: The cell thickness was measured on multiple images where neither nucleus or GVs were observed. The central part of the cell was identified by a perpendicular *red dotted line* drawn at the halfway point of a *red solid line* connecting the two cell borders. Then, a *green solid line* was drawn through the axis of the cell, intersecting the *red dotted line*. Finally, a *yellow solid line* perpendicular to the green axis line was drawn to measure cell thickness, crossing the intersection of the axis line and *red dotted line*. (**E**) Cell overlap length (OL): The measurement for the OL was made by drawing a curved line (*green*) along the cell border that lapped with the other cell border. The OL measurement was done on both borders of a cell to calculate for a mean OL value for each cell. (**B–D**: measurements were made on SBF-SEM images using ImageJ).

ments was used to calculate the mean cell width in nonnuclear areas per cell. Cell thickness was measured on SBF-SEM images at multiple locations (at least 5) along the length of the cell (every 40 sections), where no GVs or a nucleus was observed, and the average of those measurements was used to calculate mean thickness per cell (Fig. 1D).

IW/IW Connectivity. The IW/IW connectivity was defined as the amount of overlapping borders between adjacent IW cells. On SBF-SEM images, we measured the length of cell border that overlaps with the adjacent cell border (Fig. 1E), termed "overlap length (OL)." The OL was measured at multiple locations along the length of the cell (every 40 sections) and on both sides of the cell. The average of these measurements was used to calculate the mean OL per cell.

IW/JCT Connectivity. The IW/JCT connectivity in an IW cell was defined as the number of connections between an IW cell and its underlying JCT cells or extracellular matrix (ECM). The number of connections was determined by manually counting every connection per cell. For a membrane protrusion to be considered a connection, its height was required to be at least 0.3 µm above the cell body as measured on SBF-SEM images. These connections were categorized into seven types, including six types based on a previous study (types 1-6),[21] and one first described in this study (type 7) (Fig. 2). Type 1 described a cell-ECM connection between an IW cell and the JCT ECM, while types 2 to 7 described six different cell-cell connections between an IW cell and JCT cells as follows: type 2: IW cell process to JCT cell body; type 3: IW tongue-in-JCT groove; type 4: IW cell process to JCT cell process; type 5: JCT cell process to IW cell body; type 6: JCT tongue-in-IW groove. In this study, type 7 described IW body-to-JCT body connection, defined as particular areas of significant cell body contacts between IW cells and JCT cells, where the contact area was $\geq$0.5 µm^2. Two cells in the immersion-fixed group were removed from this analysis, because there were some blurry areas along the cell body that prevented accurate identification or categorization of connections and would lead to an underestimation of total number of connections per cell.

GV Density, Volume, and Shape. All of the GVs in every reconstructed cell were identified and manually outlined on every SBF-SEM image in which they appeared. The number of GVs per cell was counted. To differentiate vacuoles from pinocytotic vesicles, vesicular structures smaller than 1.0 um^3 were excluded from the vacuole count.[21,32,33] The GV volumes were autocalculated using the Volume tool in Reconstruct.

Three methods were used to evaluate the GV volume per cell. The values from these three methods were compared between cells from the immersion- and perfusion-fixed groups. In the first method, we calculated and compared the mean volume of all of the GVs between the two groups. In the second method, we identified the single largest GV in each cell, and compared the means of those largest GV volume between the two groups. In the third method, we summed the volumes of all of the GVs found in each cell to calculate summed GV volume per cell.

GVs were categorized into two general types based on their shape: rounded GVs and collapsed GVs. GVs that had a smooth, dome-shaped apical surface were categorized as

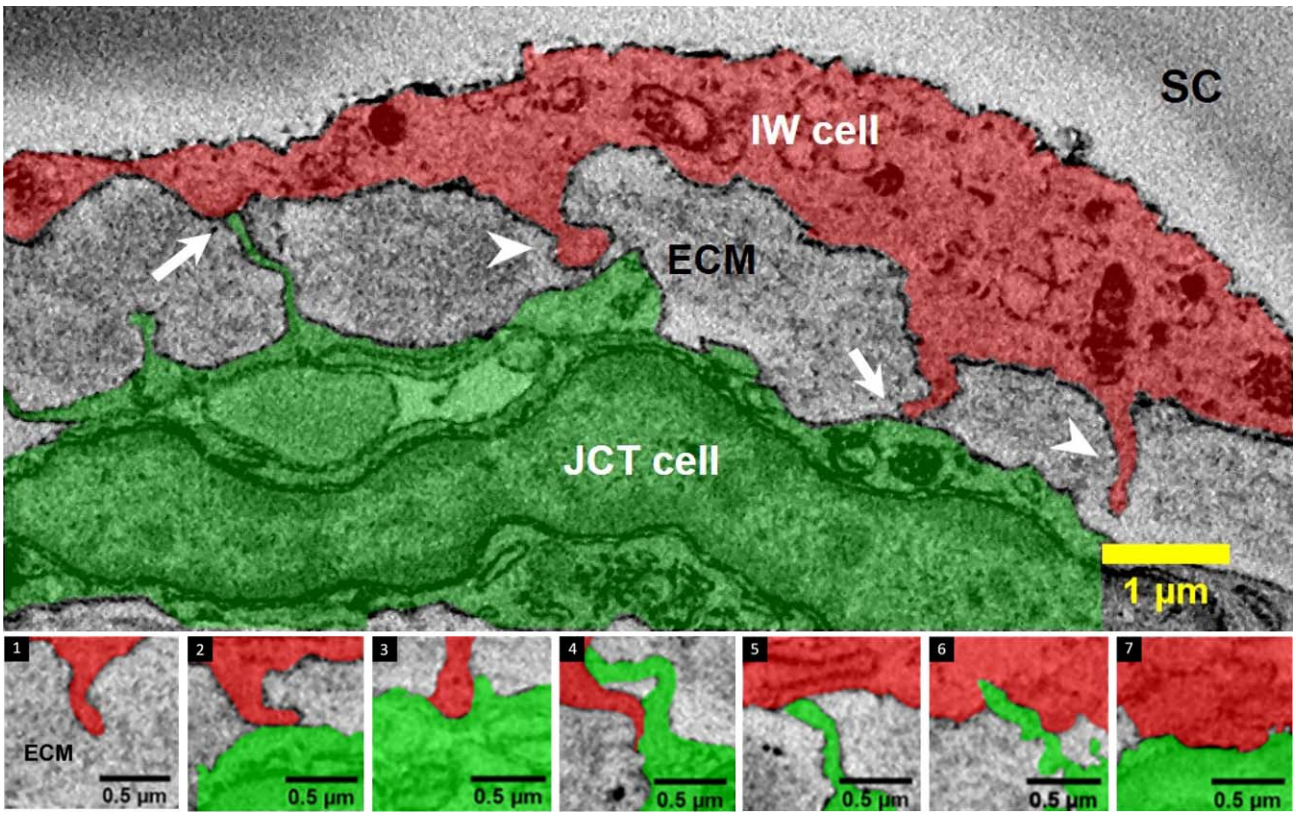

Figure 2. Types of connections between IW endothelium (*red*) of SC and underlying JCT cells (*green*)/ECM. Cell-to-cell (*arrows*) and cell-to-ECM (*arrowheads*) connections between the IW endothelium and JCT cells or ECM were categorized into seven types based on SBF-SEM images and 3D reconstructions. Type 1 shows the IW cell extending a cytoplasmic process to underlying ECM (and not to any cell bodies of JCT): Type 1: IW process-to-JCT ECM; types 2 through 7 are between an IW and JCT cell; type 2: IW process-to-JCT cell body; type 3: IW tongue-in-JCT groove; type 4: IW process-to-JCT process; type 5: JCT process-to-IW body; type 6: JCT tongue-in-IW groove, type 7: IW body-to-JCT body.

rounded GVs. GVs that had a depressed surface or indentation on the apical surface were categorized as collapsed GVs.

Identification of Pores. To identify pores, every SBF-SEM image associated with the reconstructed cells was examined (Fig. 3). I-pores were identified as elliptical openings in the cell membrane or on a GV with a smooth perimeter (Fig. 3A); B-pores were identified by smooth openings at the cell borders between two individual IW cells (Fig. 3B).[34,35] The exclusion criteria include: irregular-shaped tears, ruptures, or broken openings in the cell layer that were identified as artifacts (may occur due to tissue processing). In this study, only pores in the reconstructed IW cells were counted; we did not count the pores in non-reconstructed tissue areas.

Statistical Methods

The results from immersion- and perfusion-fixed eyes were compared to determine if there were changes in the IW/JCT connectivity, the IW/IW connectivity, GV density, GV volume and shape, and number of I- and B-pores. All statistical analyses were performed in R statistical computing package (v3.5.1; R Foundation for Statistical Computing, Vienna, Austria). Unpaired two-tailed *t*-tests were used to compare cellular dimensions with a required significance level of 0.05. We performed χ^2 analysis to test the difference in distributions of rounded and collapsed GVs between groups. Cumulative distribution frequency analysis and a nonparametric Kolmogorov-Smirnov test were used to compare the distribution of GV volumes in each group. Nonparametric Wilcoxon-rank sum tests were used to compare the GV volume between groups.

Results

IW Cell Dimensions

A total of 12 IW cells from each group were reconstructed. The mean cell length was shorter in perfusion-fixed eyes (71.88 ± 7.74 µm, mean ± SEM) than in immersion-fixed eyes (90.21 ± 5.00 µm, $P = 0.06$; Fig. 4A), but this difference did not reach significance. The mean cell width of IW cells at the nuclear area from perfusion-fixed eyes was slightly narrower than those from immersion-fixed eyes (9.74 ± 1.00 µm vs.13.29 ± 1.89 µm; $P = 0.11$; Fig. 4B), but the difference did not reach significance. The mean cell width in non-nuclear areas was significantly narrower in perfusion-fixed eyes (3.90 ± 0.41 µm) than immersion-fixed eyes (8.01 ± 0.63 µm; $P < 0.001$). The mean cell thickness of non-GV and nonnuclear regions was significantly thinner in perfusion-fixed eyes than in immersion-fixed eyes (0.58 ± 0.05 µm vs. 0.88 ± 0.01 µm; $P = 0.02$; Fig. 4C).

IW/JCT Connections

The connections between the IW cells and the JCT cells/ECM in each cell were identified, categorized, and visualized in 3D (Fig. 5). The overall IW/JCT connectivity was found to be especially substantial in immersion-fixed eyes, while it was less extensive in perfusion-fixed eyes (Fig. 5). We observed a total of 1663 connections in 22 cells, including both cell-cell and cell-ECM connections. The IW cells from immersion-fixed eyes had an average of 132 ± 20 connections (range, 46–237), and those from perfusion-fixed eyes had a significantly reduced

Investigative Ophthalmology & Visual Science

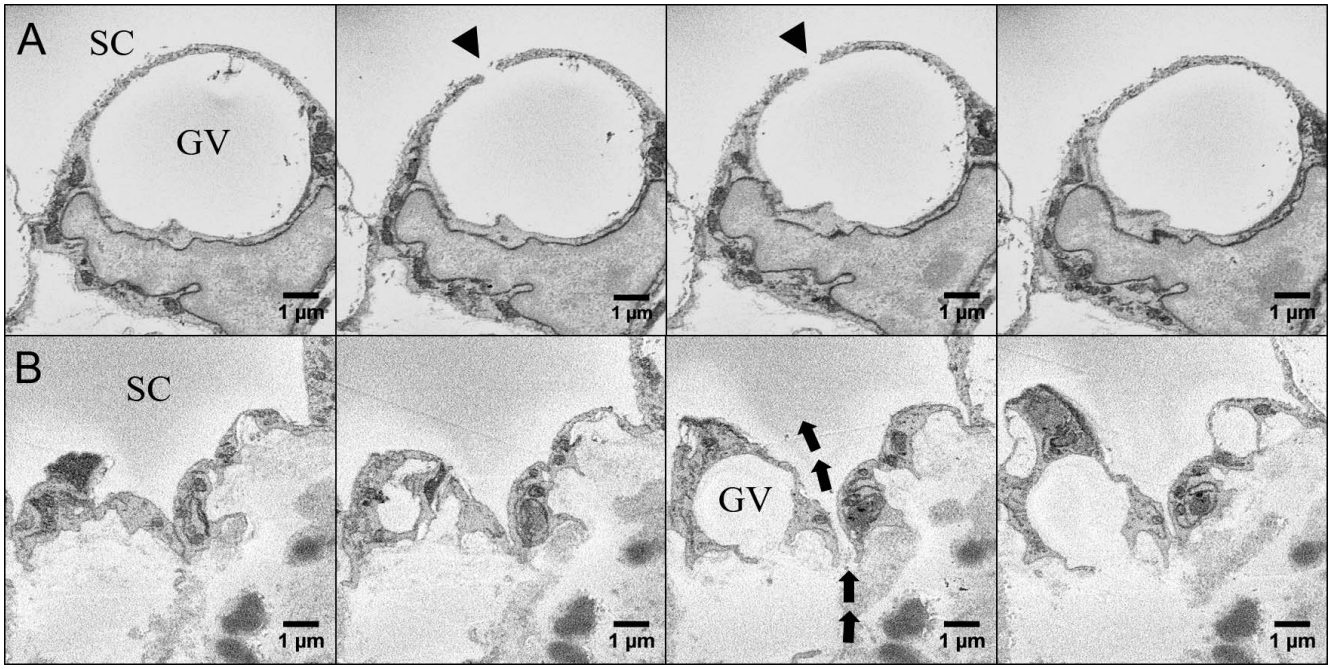

Figure 3. Serial block-face scanning electron micrographs of GV, intracellular pore (I-pore), and border pore (B-pore) in the IW endothelium of SC. (**A**) Serial images of an IW endothelial cell with a *GV* and an I-pore (*arrowhead*) leading into SC. (**B**) Serial images of a B-pore (*arrows*) located at the border between two adjacent inner wall cells of SC.

number of connections (29 ± 6; range, 6–76; $P = 0.0001$; Fig. 6A).

When only considering the connections between each IW cell and JCT ECM (not JCT cells), the IW cells from immersion-fixed eyes had an average of 50 ± 9 connections, and those from perfusion-fixed eyes had a significantly reduced number of connections (14 ± 2; $P = 0.0002$; Fig. 6B).

When only considering the connections between each IW cell and JCT cells (not JCT ECM), the IW cells from immersion-fixed eyes had an average of 81 ± 13 connections, and those from perfusion-fixed eyes had a significantly reduced number of connections (15 ± 4; $P = 0.0001$; Fig. 6C).

These connections varied in their frequencies (Fig. 6D). All but type 6 connections significantly decreased in perfusion-fixed eyes compared to immersion-fixed eyes ($P < 0.01$).

Comparison of GV Density, Volume, and Shapes

Surprisingly, we did not find a significant difference in the mean number of GVs per cell between immersion-fixed eyes (42 GVs/12 cells, 3.5 ± 0.5 GVs/cell) and perfusion-fixed eyes (41 GVs/12 cells, 3.4 ± 1.1 GVs/cell; Tables 2, 3).

When GV volume was compared between the two groups of cells using three different methods (see Methods), we found a significant increase in GV volume in the perfusion-fixed group compared to immersion-fixed group by all three methods (Fig. 7). First, mean volume of all GVs was significantly larger in perfusion-fixed eyes (144.98 ± 47.65 μm^3), compared to the immersion-fixed eyes (27.18 ± 7.09 μm^3; $P < 0.02$; Fig. 7A). Second, the mean volume of the largest GV in individual IW cells was significantly larger in perfusion-fixed eyes (437.75 ± 129.47 μm^3), compared to immersion-fixed eyes (76.51 ± 18.07 μm^3; $P < 0.02$; Fig. 7B).

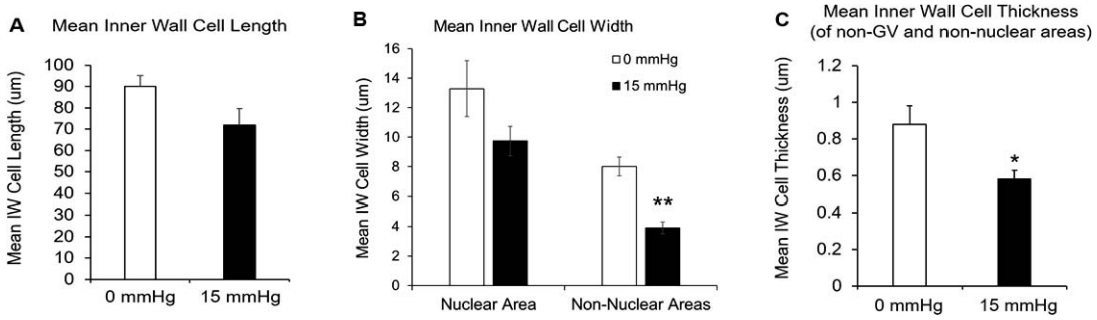

Figure 4. Comparison of cell length, width, and thickness between immersion-fixed group (0 mm Hg, $n = 12$ cells) and perfusion-fixed group (15 mm Hg, $n = 12$ cells). (**A**) The mean cell length of IW cells from perfusion-fixed eyes was shorter than those from immersion-fixed eyes (71.88 ± 7.74 µm vs. 90.21 ± 5.00 µm; $P = 0.06$), but the difference did not reach significance. (**B**) The mean cell width of IW cells at the nuclear area from perfusion-fixed eyes was slightly narrower than those from immersion-fixed eyes (9.74 ± 1.00 µm vs.13.29 ± 1.89 µm), but the difference did not reach significance ($P = 0.11$). The mean cell width in non-nuclear areas was significantly narrower in perfusion-fixed eyes (3.90 ± 0.41 µm) than immersion-fixed eyes (8.01 ± 0.63 µm; $P < 0.001$). (**C**) The mean cell thickness of non-GV and non-nuclear regions was significantly thinner in perfusion-fixed eyes than in immersion-fixed eyes (0.58 ± 0.05 µm vs. 0.88 ± 0.01 µm; $P = 0.02$). *Error bars:* SEM. $^*P \leq 0.05$; $^{**}P \leq 0.01$.

Investigative Ophthalmology & Visual Science

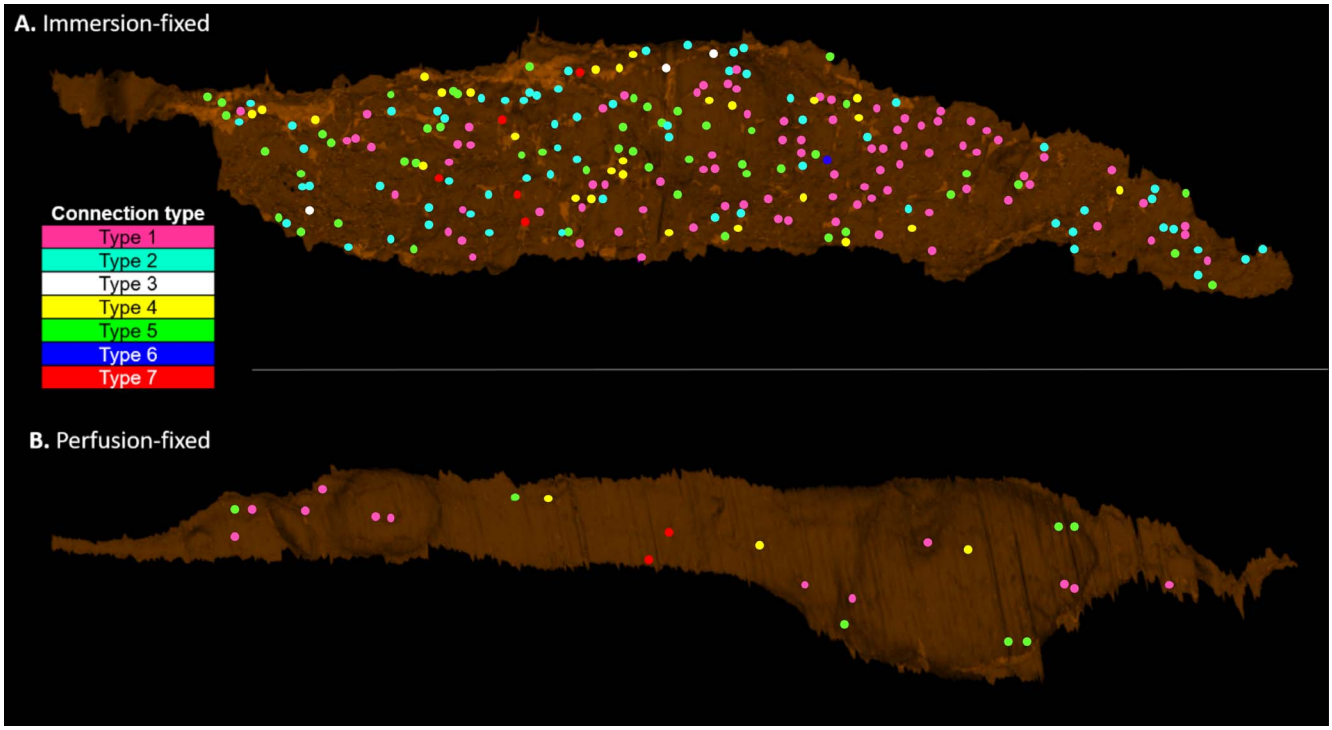

FIGURE 5. Comparison of IW/JCT connectivity between immersion- and perfusion-fixed tissues. One IW cell from each group was shown here as an example (*basal view*). In each cell, the cell body was 3D-reconstructed, and all of the IW/JCT cell-cell and cell-ECM connections were identified and visualized as well. (**A**) IW cell from immersion-fixed eyes. (**B**) IW cell from perfusion-fixed eyes. The seven types of connections were color coded. Type 1: *pink*; type 2: *light blue*; type 3: *white*; type 4: *yellow*; type 5: *green*; type 6: *dark blue*; type 7: *red*.

Third, the mean summed GV volume in individual IW cells was significantly larger in perfusion-fixed eyes (495.36 ± 134.21 μm^3), compared to immersion-fixed eyes (95.12 ± 19.45 μm^3; $P < 0.01$; Fig. 7C).

In both the immersion- and perfusion-groups, there were a higher percentage of rounded GVs (73.81% and 87.80%) compared to collapsed GVs (26.19% and 12.20%, respectively). However, the percentage of rounded GVs was higher in the perfusion-fixed group compared to immersion-fixed group (87.80% vs. 73.81%; Fig. 8A). The rounded GVs were significantly larger in perfusion-fixed tissues compared to immersion-fixed tissues (135.06 ± 50.35 μm^3 vs. 21.67 ± 7.83 μm^3, $P = 0.04$; Fig. 8B). In immersion-fixed tissues, the collapsed GVs were larger in volume compared to the rounded GVs, but this difference did not reach significance (42.88 ± 15.31 μm^3 vs. 21.67 ± 7.83 μm^3, $P = 0.19$). Similarly, in perfusion-fixed tissues, the collapsed GVs were larger in volume compared to the rounded GVs, but the difference did not reach significance (261.47 ± 158.10 μm^3 vs. 135.06 ± 50.35 μm^3, $P = 0.58$). χ^2 test with Yates correction showed that the association between fixation conditions and GV shapes was not statistically significant ($\chi^2 = 0.515$; $P = 0.47$).

GVs and I-Pores

A total of six I-pores were found from six individual GVs out of the 41 GVs in 12 cells from perfusion-fixed eyes (Table 3; Fig. 9). No I-pores were observed from 42 GVs in 12 cells from immersion-fixed eyes (Table 2). The cumulative distribution frequency (CDF) is shown for GV volume distribution in Figure 10. The CDF was not different between immersion-fixed GVs and perfusion-fixed GVs without pores ($P = 0.33$). There were too few pores to compare via Kolmogorov-Smirnov test for perfusion-fixed GVs with pores; however, there is a clear shift to the right toward larger GV volumes compared to the other two distributions. In perfusion-fixed eyes, there was a higher percentage of GVs whose volumes were greater than 100 μm^3, compared to immersion-fixed eyes (26.8% vs. 9.5%). The smallest GV that had an I-pore was 41.72 μm^3. All of the I-pores observed were associated with rounded GVs.

IW/IW Connectivity and B-Pores

A total of 2 B-pores were found in the perfusion-fixed group, while no B-pores were observed in immersion-fixed eyes. Through examining B-pores on the SBF-SEM images in ImageJ and in 3D-EM reconstructed scenes in Reconstruct, we found that B-pores were only found in areas along the cell border where the amount of connectivity between adjacent IW cells was minimized to zero (overlap length [OL] = 0 μm; Figs. 11A–C), and the sections immediately before and after the B-pore still showed minimal cell overlap (OL < 0.5 μm). The mean IW/IW overlap length significantly decreased in cells from perfusion-fixed eyes compared to immersion-fixed eyes (OL = 0.93 ± 0.24 μm vs. 1.63 ± 0.12 μm, $P < 0.01$; Fig. 11D).

DISCUSSION

In this study, using SBF-SEM and 3D reconstruction, we investigated IW/JCT and IW/IW connectivity and their potential roles in GV and pore formation by comparing the IW cells from perfusion-fixed eyes to those from immersion-fixed eyes. Our main findings were:

1. Mean number of IW/JCT cell-cell connections per cell decreased, while summed GV volume per cell increased in perfusion-fixed eyes compared to immersion-fixed eyes;

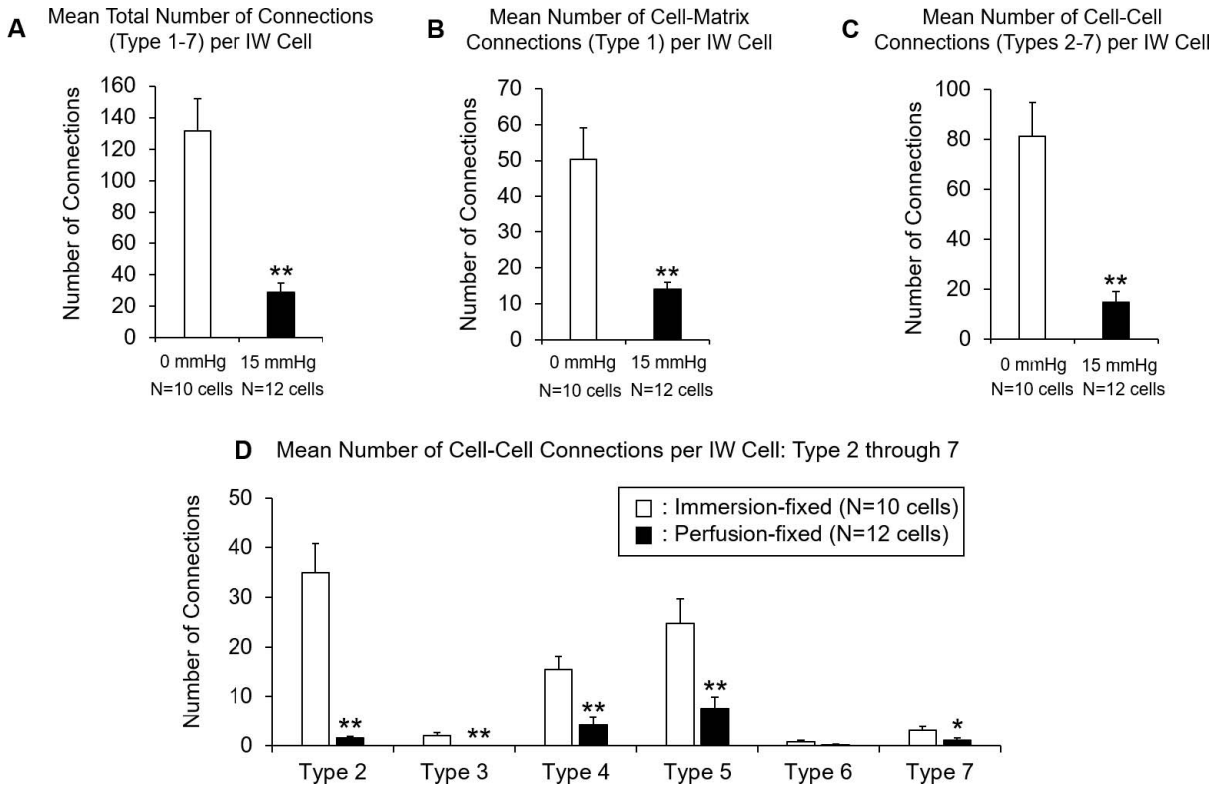

Figure 6. Comparison of mean number of connections in each IW cell to underlying JCT cells/ECM between perfusion-fixed ($n = 12$ cells) and immersion-fixed ($n = 10$ cells) eyes. (**A**) Mean total number of IW/JCT connections (sum of type 1-type 7) was significantly reduced in perfusion-fixed eyes (29 ± 6 connections), compared to immersion-fixed eyes (132 ± 20 connections; $P = 0.0001$). (**B**) Mean number of cell-to-ECM connections (type 1 only) between each IW cell with underlying JCT ECM was significantly reduced in perfusion-fixed eyes (14 ± 2 connections), compared to immersion-fixed eyes (50 ± 9 connections; $P = 0.0002$). (**C**) Mean number of cell-to-cell connections (types 2–7 altogether) between each IW cell with JCT cell bodies was significantly reduced in perfusion-fixed eyes (15 ± 4 connections), compared to immersion-fixed eyes (81 ± 13 connections; $P = 0.0001$). (**D**) Mean numbers of six different types of cell-to-cell connections between each IW cell and JCT cells are shown. All but type 6 connections were significantly reduced in perfusion-fixed eyes, compared to immersion-fixed eyes ($P < 0.01$). *Error bars*: SEM. $^{*}P \leq 0.05$; $^{**}P < 0.01$.

2. There was no difference in GV density per cell between immersion- and perfusion-fixed eyes;
3. No pores were observed in immersion-fixed eyes, while 14.6% of GVs had I-pores in perfusion-fixed eyes (I-pores only in GVs larger than 41.72 μm^3);
4. In perfusion-fixed eyes, the mean IW/IW overlap length per cell decreased significantly, and B-pores were found only in regions where IW/IW overlap length became zero.

These results support our hypothesis that larger GVs in perfusion-fixed eyes are associated with a decrease in IW/JCT connectivity and increased I-pore formation and that a decrease in IW/IW connectivity may promote B-pore formation, and thus may contribute to the regulation of aqueous outflow resistance. Although previous studies suggest that the pores, on their own, may only generate 10% of outflow resistance,[36] a hydrodynamic interaction between the pores of the IW of SC and the underlying JCT may greatly increase outflow resistance in this region through a "funneling effect" by confining the flow to the JCT regions near the IW pores, forcing a funneling pattern of aqueous outflow; thus, pores may modulate the resistance in this region.[37]

SBF-SEM provided serial, high-resolution images across a substantial volume of tissues. Combined with 3D reconstruction, this method overcomes the limitations of 2D imaging and enabled us for the first time to quantify accurately the IW/JCT and IW/IW connectivity, to determine GV volume, density, shape, and pores per IW cell, and to compare their differences between immersion- and perfusion-fixed tissues.

Grierson et al.[21] characterized 6 types of IW/JCT connections. They examined a total of 1000 randomly-selected IW/JCT connections in the IW endothelium of nine rhesus monkey eyes and described the IW/JCT cell-cell connections as desmosomes capable of sustaining cellular stress in the direction of outflow. However, the study was unable to document how extensive the IW/JCT connectivity was at the level of individual cells and how this connectivity changes under different pressure gradients. In the current study, we collected serial, high-resolution images through the entire tissue blocks (each block was $134 \times 59 \times 187$ μm^3 on average; see Table 1), which captured all of the 1663 IW/JCT connections in 22 entirely reconstructed IW cells. We were able to detect an additional type of IW/JCT cellular connection, IW cell body-JCT cell body connection. We demonstrated, for the first time to our knowledge, that the IW/JCT connectivity was extremely substantial in IW cells of immersion-fixed eyes, and the overall IW/JCT connectivity was significantly decreased in IW cells of perfusion-fixed eyes.

We found that along with decreased IW/JCT connectivity, the IW cells became shorter, significantly narrower in nonnuclear regions, and significantly thinner in perfusion-fixed eyes. IW cells are thought to respond to the pressure gradient in the form of mechanical stretch or distortion of the outflow resistance through changes in the ECM composition as well as cellular cytoskeletal organization.[38,39] Previous studies

Table 2. Summary of GV Volumes and I-Pores in Reconstructed IW Cells From Immersion-Fixed (0 mm Hg) Eyes

Donor ID	Inner Wall Cell Number	Giant Vacuole Number	Volume, μm^3	I-Pore Count
Eye 01	Cell 1	1	71.03	0
		2	7.06	0
		3	1.89	0
		4	1.87	0
		5	1.59	0
		6	1.07	0
	Cell 2	1	46.94	0
		2	4.47	0
		3	4.13	0
		4	1.33	0
	Cell 3	1	152.28	0
		2	5.89	0
		3	1.00	0
Eye 02	Cell 4	1	12.07	0
		2	10.13	0
		3	2.08	0
		4	1.24	0
	Cell 5	1	59.13	0
		2	13.76	0
		3	12.55	0
		4	5.28	0
		5	3.01	0
		6	2.03	0
	Cell 6	1	119.19	0
		2	12.83	0
		3	11.13	0
		4	7.07	0
		5	3.86	0
		6	2.05	0
	Cell 7	1	15.32	0
		2	2.59	0
	Cell 8	1	8.61	0
	Cell 9	1	209.99	0
		2	15.15	0
	Cell 10	1	82.99	0
		2	49.53	0
	Cell 11	1	26.24	0
		2	12.60	0
		3	5.03	0
		4	1.61	0
	Cell 12	1	114.33	0
		2	19.46	0

Table 3. Summary of GV Volumes and I-Pores in Reconstructed IW Cells From Perfusion-Fixed (15 mm Hg) Eyes

Donor ID	Inner Wall Cell Number	Giant Vacuole Number	Volume, μm^3	I-Pore Count
Eye 03	Cell 1	1	1419.76	1
		2	116.59	0
	Cell 2	1	824.02	0
	Cell 3	1	234.23	0
		2	12.96	0
Eye 04	Cell 4	1	117.09	1
		2	87.95	0
		3	51.07	1
		4	18.63	0
		5	8.34	0
		6	5.99	0
		7	3.92	0
		8	3.27	0
		9	2.25	0
		10	2.24	0
		11	2.12	0
		12	2.00	0
		13	1.58	0
		14	1.40	0
		15	1.17	0
	Cell 5	1	423.55	0
		2	81.62	0
		3	5.51	0
		4	3.17	0
		5	1.24	0
	Cell 6	1	1041.62	1
		2	4.92	0
		3	4.19	0
	Cell 7	1	530.87	0
		2	201.87	0
	Cell 8	1	429.80	1
		2	11.59	0
	Cell 9	1	41.72	1
		2	8.74	0
	Cell 10	1	55.97	0
	Cell 11	1	21.81	0
		2	13.94	0
		3	9.64	0
		4	6.47	0
	Cell 12	1	112.61	0
		2	16.91	0

have also shown that many IW cells possess a large reservoir of excess membrane stored in ruffles, folds, or vesicles[40,41] that allow the cell to rapidly change shape without altering the total membrane surface area.[9,42] It is possible that with the physical detachment of IW cells from the underlying JCT, IW cells become more capable of deforming along the pressure gradient, forming larger outpouchings (GVs) into SC. The newly available cell membrane that initially made up the surface area of the original cellular connections may be recruited to help the cell body deform, and thereby form larger GVs. In this study, we tested the relationship between the number of IW/JCT cell-cell connections and the summed GV volume in each group, but did not find a linear relationship (perfusion-fixed: $R^2 = 0.098$; $n = 10$; $P > 0.05$); immersion-fixed: $R^2 = 0.044$; $n = 12$; $P > 0.05$). This suggests that in addition to IW/JCT cell-cell connections, other factors may influence GV volume, such as active and inactive flow regions, IOP/perfusion-pressure, cell and ECM stiffness, and these warrant further investigation.

We determined the exact number of GVs in each reconstructed cell and found that there were often multiple GVs per IW cell, and usually one large GV was accompanied by a few smaller GVs. We also found no significant difference in the total number of GVs per IW cell between the immersion- and perfusion-fixed groups, which was an interesting finding. Previous studies showed that to study GVs, perfusion-fixation is necessary, because GVs are pressure-dependent structures.[21,32,43–45] Another study also showed that after ocular perfusion was halted, 70% of GVs disappeared in 3 minutes.[45] In our study, although the GV density per cell was not significantly different between the two groups, the mean GV volume was significantly smaller, and there was a higher percentage of smaller GVs in immersion-fixed eyes. This suggests that the GVs in immersion-fixed eyes were deflating gradually, but did not disappear completely, during the 24-hour

Investigative Ophthalmology & Visual Science

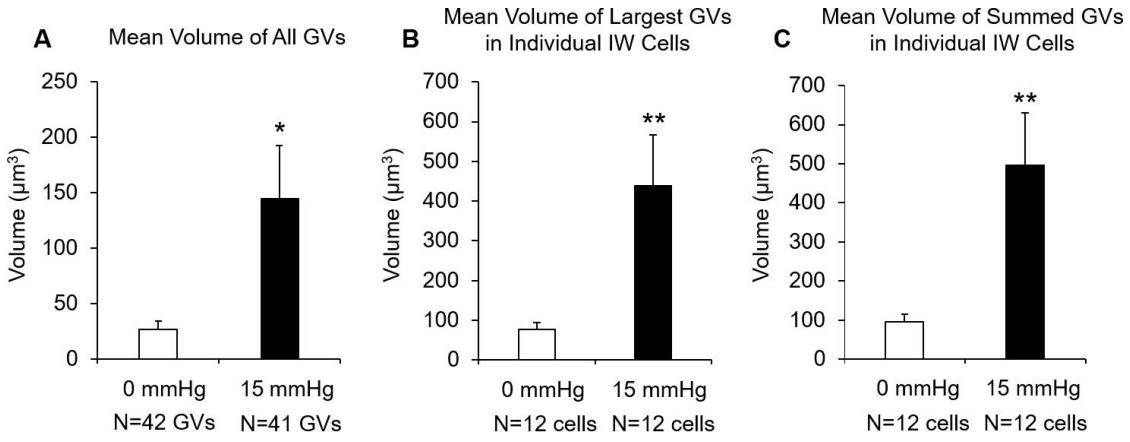

Figure 7. A comparison of GV volume between immersion-fixed eyes ($n = 12$ cells, 42 GVs) and perfusion-fixed eyes ($n = 12$ cells, 41 GVs). (**A**) The mean volume of all GVs was significantly larger in perfusion-fixed eyes (144.98 ± 47.65 μm^3), compared to the immersion-fixed eyes (27.18 ± 7.09 μm^3; $P < 0.02$). (**B**) Mean volume of the largest GVs in individual IW cells was significantly larger in perfusion-fixed eyes (437.75 ± 129.47 μm^3), compared to immersion-fixed eyes (76.51 ± 18.07 μm^3; $P < 0.02$). (**C**) Mean of summed GV volume in individual IW cells significantly larger in perfusion-fixed eyes (495.36 ± 134.21 μm^3) compared to immersion-fixed eyes (95.12 ± 19.45 μm^3; $P < 0.01$). *Error bars*: SEM. *$P \leq 0.05$; **$P < 0.01$.

postmortem period as well as during a couple of minutes when a small cut was made in the eyes to be immersion-fixed immediately after. Additionally, since the GVs in immersion-fixed eyes were smaller and tended to span fewer serial images than larger GVs in perfusion-fixed eyes, these small GVs could have been easily missed if only one random cross-sectional image of SC was examined using traditional 2D imaging. This may have led to an underestimation of GV count/density in immersion-fixed tissues in previous studies.[33] In order to confirm this, we did additional investigation and comparison between GV density per cell in random TEM sections from eyes with immersion-fixed versus perfusion-fixed at 15 mm Hg from a previous study.[22] Four eyes were immersion-fixed, and four were perfusion-fixed at 15 mm Hg. The fixation methods were similar as those in the current paper. TEM images were taken randomly along the IW of SC of each eye. We analyzed 78 (at least 17 per eye) images containing 475 IW cells for immersion-fixed eyes and found 31 GVs. In perfusion-fixed eyes, we analyzed 88 images containing 803 IW cells and found 329 GVs. We found that the mean percentage of cells with GV in immersion-fixed eyes was much lower than that in 15 mm Hg (6.7% vs. 47.4%; 0.16 versus 1.46/μm of SC), compared to the similar density found between two groups in our current study with SBF-SEM and 3D reconstruction. Our data suggest that even when observing hundreds of cells at each pressure with similar fixation methods, 2D studies of random sections still can not provide a true picture of GV presence per cell.

However, GV density observed in immersion-fixed eyes could vary due to preparation methods. A previous study by Grierson and Lee reported that no GVs were found at 0 mm Hg when eyes were rapidly immersed in fixative without a cut along the equator.[33] Brilakis and Johnson[45] hemisected eyes and cut the anterior segment into 6 wedges before immersion in fixative and reported 70% decrease in GV counts after 3 minutes, 82% decrease after 15 minutes, and 88% decrease by 120 minutes after discontinuation of saline perfusion at 20 or

A

Shape category	Rounded	Collapsed
3D-reconstruction and SBF-SEM of GV	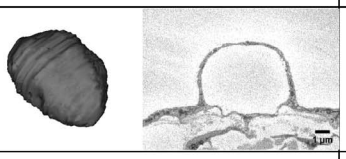	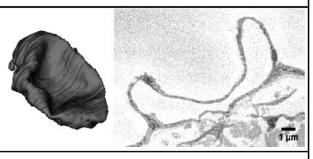
GV count (in %), 0 mmHg	31 (73.81%)	11 (26.19%)
GV count (in %), 15 mmHg	36 (87.80%)	5 (12.20%)

B

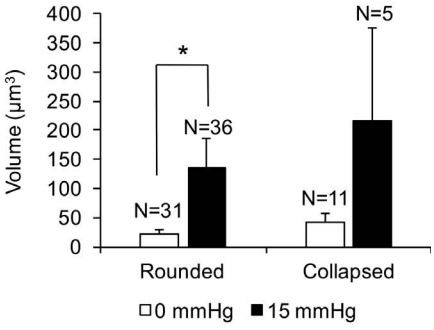

Figure 8. A comparison of two types of shapes (rounded, collapsed) of GVs in immersion-fixed (0 mm Hg) and perfusion-fixed (15 mm Hg) eyes. (**A**) In both groups, there were a higher percentage of rounded GVs than collapsed GVs. However, the percentage of rounded GVs was higher in perfusion-fixed eyes compared to immersion-fixed eyes. (**B**) The rounded GVs were significantly larger in perfusion-fixed eyes compared to immersion-fixed eyes (135.06 ± 50.35 μm^3 vs. 21.67 ± 7.83 μm^3, $P = 0.04$). In immersion-fixed tissues, the collapsed GVs were larger compared to the rounded GVs, but the difference did not reach significance (42.88 ± 15.31 μm^3 vs. 21.67 ± 7.83 μm^3, $P = 0.192$). Similarly, in perfusion-fixed eyes, the collapsed GVs were larger compared to the rounded GVs, but the difference did not reach significance (261.47 ± 158.10 μm^3 vs. 135.06 ± 50.35 μm^3, $P = 0.583$).

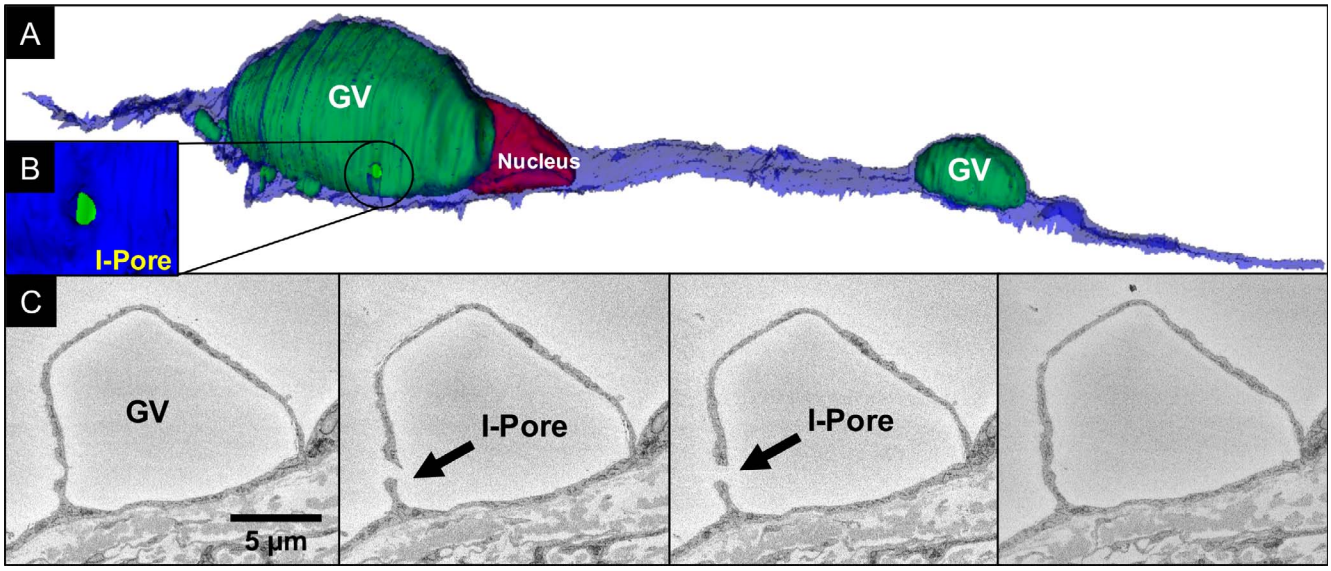

FIGURE 9. 3D scene of an IW endothelial cell with two GVs and a pore. (**A**) An IW cell (*blue*) with an I-pore (*circled*) associated with one of two GVs (*green*) near nucleus (*dark red*) was reconstructed based on serial, ultrathin scanning EMs. (**B**) Higher magnification snapshot of the reconstructed I-pore encircled in (**A**). (**C**) Four serial block-face scanning electron micrographs from which the I-pore (*arrow*) and GV were reconstructed.

40 mm Hg when compared with perfusion-fixed fellow eyes at same pressure.[45] In our method, we made a small cut along the equator before immersion in fixative; this procedure may cause a pressure spike. However, the pressure influence in our preparation would be smaller than that in Brilakis and Johnson's method with hemisecting eyes. We observed an 89% decrease in GV counts in our immersion-fixed eyes compared to perfusion-fixed eyes at 15 mm Hg by analysis of the images from our previous study with same preparation method,[22] which is similar to the 88% decrease in GV counts after 120 minutes reported by Brilakis and Johnson.[45] Unlike Brilakis and Johnson's method, who placed tissue wedges in the fixative and thus fixation was nearly immediate, we placed the whole eye with a small cut along the equator into the

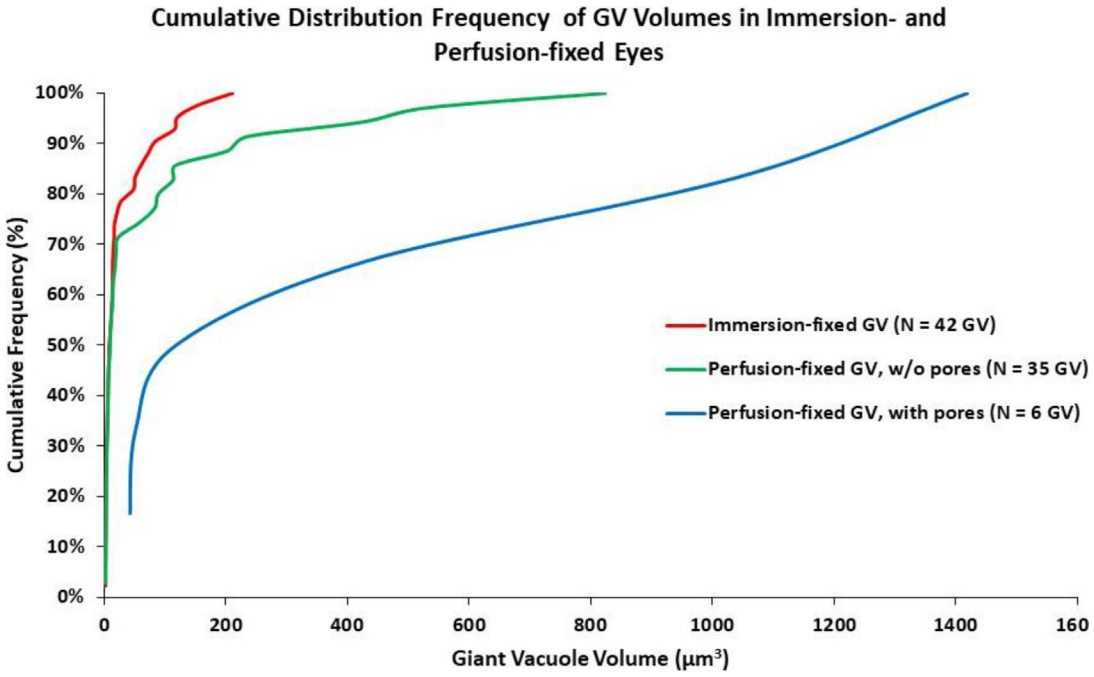

FIGURE 10. Cumulative distribution frequencies of GV volumes in immersion- and perfusion-fixed eyes. Cumulative distribution frequencies were not different between immersion-fixed GVs and perfusion-fixed GVs without pores ($P = 0.33$). There is a clear shift to the right toward larger GV volumes in perfusion-fixed GVs with pores compared to the other two distributions. In perfusion-fixed samples, I-pores were only observed in GVs larger than 41.72 μm^3.

Investigative Ophthalmology & Visual Science

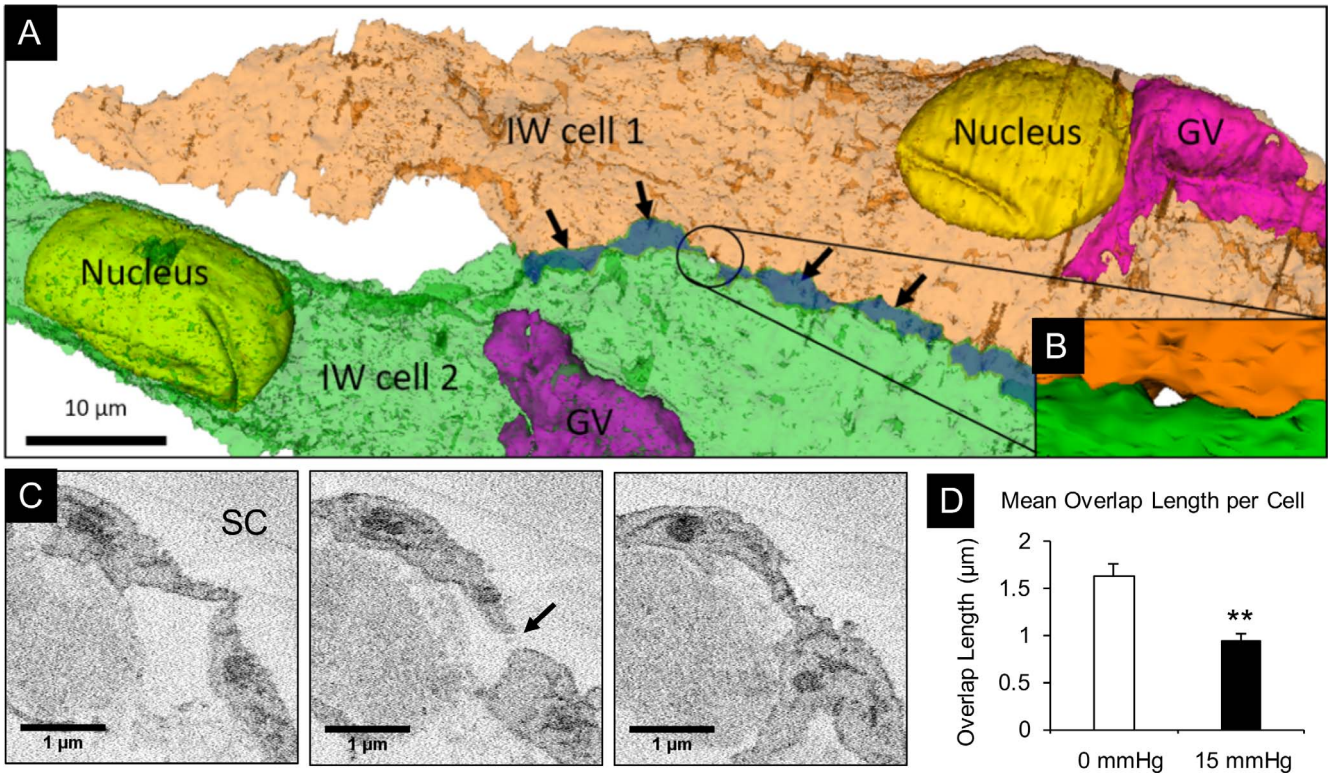

Figure 11. Analysis of B-pores and overlapping cell margins between two IW cells. (**A**) Two adjacent IW cells (*green* and *orange*) were made semitransparent to show overlapping cell margins (*dark green region* indicated by *arrows*) and a B-pore (*encircled*). (**B**) Higher magnification snapshot of reconstructed pore encircled in (**A**). (**C**) Three serial block-face scanning electron micrographs from which the B-pore (*arrow*) was identified and reconstructed. (**D**) Comparison of the mean overlap length (OL) in IW cells from immersion-fixed eyes ($n = 12$ cells) and perfusion-fixed eyes ($n = 12$ cells). Mean OL was significantly less in perfusion-fixed eyes (0.93 ± 0.24 µm) compared to immersion-fixed eyes (1.63 ± 0.12 µm; $P < 0.01$). *Error bars*: SEM. $^{**}P < 0.01$.

fixative. It would take a longer time for fixative to diffuse to SC from the equator than across the sclera. The vacuoles would not be fixed until the fixative diffuses across the sclera and reaches the inner wall of SC. Given that the thickness of the sclera is about 1 mm, and using a diffusion coefficient of glutaraldehyde in polymer networks of 3×10^{-6} cm^2/sec,[46] we estimate that it will take roughly 15 to 30 minutes before a significant concentration of glutaraldehyde reaches the inner wall of SC. Another difference was that the perfusion pressure was higher in Brilakis and Johnson's study, and thus GVs in their study might be larger before fixation than that in our study.[32,33] Our current study focuses on comparison of GVs between 2D and 3D methods using the same fixation preparation.

Grierson and Lee[33] calculated the theoretical GV volume (16.71 µm^3, 15 mm Hg, based on a spheroidal model of GV shape) from measurements from the light micrograph with the largest cross-sectional area of each GV (section thickness = 1.5 µm). Their GV volume in monkey eyes calculated from light micrographs was significantly smaller compared to our GV volume in human eyes observed via SBF-SEM and 3D reconstruction (144.98 ± 47.65 µm^3, $n = 41$ GVs, 15 mm Hg; one-sample t-test, $P = 0.01$). We calculated the theoretical GV volume using Grierson and Lee's method and a small number of GVs ($n = 10$) from our study by selecting the largest cross-sectional area of each GVs and several random cross-sectional areas away from the largest. Our analysis revealed that theoretical GV volume calculated from a random cross-sectional area was different than its true 3D-calculated GV volume by 29% to 98% depending on the distance from the largest cross-sectional area of that GV. Our results suggest that a single cross-sectional image of GV may not be representative of its true size, because in most cases the cross-sectional area is not imaged at the location where the GV is the largest, which may result in an underestimation or overestimation of its true size.

We found relatively more rounded GVs and fewer collapsed GVs in the perfusion-fixed group. Because the immersion-fixed eyes were without active outflow for less than 24 hours and a small cut was made at the equator of the eyes before immediate immersion-fixation upon their delivery to our laboratory, we speculated that many of the GVs observed were beginning to deflate due to the dissipation of IOP, resulting in fewer rounded GV. This may explain why more GVs appeared as if they were on their way to collapse or deflate in immersion-fixed samples, whereas more GVs appeared rounded in perfusion-fixed samples.

The technique of SBF-SEM followed by 3D reconstruction is advantageous in studying pores, because reconstructed cells could be freely rotated to any viewpoint so that even pores obstructed by surrounding structures could be observed. If traditional scanning or transmission electron microscopy were used, some pores could have been obstructed in en face imaging, or not imaged at all due to the lack of serial images. One previous study using random TEM imaging reported only 1.6% of GV had luminal pores at the same perfusion pressure.[47] In this study, a total of 6 I-pores (14.6%) were found in 12 inner wall cells from the perfusion-fixed eyes. This percentage is consistent with previous studies using SEM that found 13% to 29% of GVs to have pores,[48,49] but falls on the lower end of the

range. This may be due to nonuniform distribution of pores along the inner wall endothelium,[20] and we might have used IW endothelial tissues from regions with lower pore density. This may be related to the segmental nature of aqueous humor outflow through the trabecular meshwork.[14,50–52] Future studies using 3D-EM to identify pores across a larger surface area of IW endothelium in active and inactive outflow regions are warranted.

All 6 of the I-pores observed in this study were associated with rounded GVs larger than 41.72 μm^3. Using 41.72 μm^3 as a threshold, we found that the perfusion-fixed group had relatively more GVs that were larger than this size compared to the immersion-fixed group (39% vs. 21%) (Fig. 10; Tables 2, 3). Since we only investigated a small number of cells in this study, further study using a larger sample size is needed to confirm our finding. In addition, it seems that GV volume is not the only contributing factor for pore formation, as shown by our finding that not all GVs larger than 41.72 μm^3 formed pores. In the perfusion-fixed group, only 37.5% (6 out of 16) of larger GVs (size >41.72 μm^3) formed pores; furthermore, in the immersion-fixed group, none of these larger GVs formed pores. This suggests that a large GV volume itself may not guarantee pore formation. Although mean volumes of the collapsed GVs were larger than rounded GVs, no I-pores were observed associated with collapsed GVs, suggesting that tension or strain of a GV may also play a role in pore formation. This finding is consistent with a previous study that reported increasing biomechanical strain acted as a trigger for pore formation in cultured SC cells.[53]

SBF-SEM followed by 3D reconstruction enhanced our ability to quantify B-pores and study their surrounding environment. Two B-pores were found in the perfusion-fixed eyes, while none were observed in immersion-fixed eyes. Our observations in perfusion-fixed eyes of: 1) decreased IW/IW cell overlap length, and 2) B-pores were found only in regions where IW/IW overlap length became zero, suggest that decreased IW/IW connectivity may promote B-pore formation. Previous studies showed that pore formation may be influenced by biomechanical strain on the IW cells. IW cells have been thought to be able to regulate pore density based on biomechanical cues in the immediate environment through changing their own cell stiffness and gene expression.[53] Therefore, it is possible that tight junctions between adjacent IW cells are responsive to changing physiological conditions, which is a potential mechanism that regulates the reduced amount of cell-cell overlap, resulting in changes in local filtration characteristics of the IW endothelium. Our study on B-pore formation was limited by a small number of cells that we were able to reconstruct in a reasonable amount of time. Future studies are needed to investigate pores across larger surface areas of IW endothelium.

SBF-SEM followed by 3D reconstruction studies are generally time-consuming and labor-intensive. Our study examined over 7000 SBF-SEM images and completed thousands of tracings for cells and organelles, and we were only able to study a total of 24 cells in great detail. SBF-SEM is also limited to imaging of fixed tissues. Our study was unable to determine the stage at which each GV was observed during GV formation. There was also no way to determine whether the GVs without I-pores simply did not form pores, had formed pores moments before, or were on the way to develop pores. Future studies using live cell imaging and time-lapse microscopy may provide new insight into the dynamic process of GV and pore formation. Since there is no episcleral venous pressure in enucleated human donor eyes, our perfusion pressure at 15 mm Hg represents a higher pressure drop across the outflow pathway than the physiologic pressure in normal living eyes; therefore, the measured effects may be somewhat magnified compared to in vivo physiologic pressure.

In summary, while SBF-SEM and 3D-EM reconstruction were labor and time intensive, a major advantage of the technique was that the serial, high-resolution imaging allowed us to study cellular connectivity in a 3D space, while providing volumetric data. With this technique, we demonstrated that the IW/JCT cell-cell connectivity significantly reduced and the summed GV volume per cell significantly increased in perfusion-fixed eyes. The IW/IW connectivity (cell overlap) significantly decreased in perfusion-fixed eyes, which may increase the possibility of B-pore formation. Our findings suggest that IW/JCT and IW/IW connectivity may play a role in regulating aqueous outflow through modulating the size of GVs and number of pores. Therefore, targeting and modifying IW/JCT and IW/IW connectivity may be used as a strategy to develop potential therapeutics to regulate outflow resistance and IOP.

Acknowledgments

The authors thank Emily Benson and Grahame Kidd, PhD, of Renovo Neural, Inc. for the technical assistance and Mark Johnson, PhD, for discussion.

Supported by BrightFocus Foundation (2016099), NIH/NEI EY022634, EY019696, and The Massachusetts Lions Eye Research Fund.

Disclosure: **J. Lai**, None; **Y. Su**, None; **D.L. Swain**, None; **D. Huang**, None; **D. Getchevski**, None; **H. Gong**, None

References

1. Quigley HA. Number of people with glaucoma worldwide. *Br J Ophthalmol*. 1996;80:389–393.
2. Nemesure B, Honkanen R, Hennis A, Wu SY, Leske MC; Barbados Eye Study Group. Incident open-angle glaucoma and intraocular pressure. *Ophthalmology*. 2007;114:1810–1815.
3. The Advanced Glaucoma Intervention Study (AGIS): 7. The relationship between control of intraocular pressure and visual field deterioration. The AGIS Investigators. *Am J Ophthalmol*. 2000;130:429–440.
4. Grant WM. Clinical measurements of aqueous outflow. *AMA Arch Ophthalmol*. 1951;46:113–131.
5. Grant WM. Further studies on facility of flow through the trabecular meshwork. *AMA Arch Ophthalmol*. 1958;60:523–533.
6. Grant WM. Experimental aqueous perfusion in enucleated human eyes. *Arch Ophthalmol*. 1963;69:783–801.
7. Mäepea O, Bill A. The pressures in the episcleral veins, Schlemm's canal and the trabecular meshwork in monkeys: effects of changes in intraocular pressure. *Exp Eye Res*. 1989;49:645–663.
8. Mäepea O, Bill A. Pressures in the juxtacanalicular tissue and Schlemm's canal in monkeys. *Exp Eye Res*. 1992;54:879–883.
9. Overby DR, Stamer WD, Johnson M. The changing paradigm of outflow resistance generation: towards synergistic models of the JCT and inner wall endothelium. *Exp Eye Res*. 2009;88:656–670.
10. Johnson M, Chan D, Read AT, Christensen C, Sit A, Ethier CR. The pore density in the inner wall endothelium of Schlemm's canal of glaucomatous eyes. *Invest Ophthalmol Vis Sci*. 2002;43:2950–2955.
11. Lütjen-Drecoll E. Structural factors influencing outflow facility and its changeability under drugs. A study in Macaca arctoides. *Invest Ophthalmol*. 1973;12:280–294.

12. Rao PV, Deng PF, Kumar J, Epstein DL. Modulation of aqueous humor outflow facility by the Rho kinase-specific inhibitor Y-27632. *Invest Ophthalmol Vis Sci*. 2001;42:1029–1037.
13. Lu Z, Overby DR, Scott PA, Freddo TF, Gong H. The mechanism of increasing outflow facility by rho-kinase inhibition with Y-27632 in bovine eyes. *Exp Eye Res*. 2008; 86:271–281.
14. Lu Z, Zhang Y, Freddo TF, Gong H. Similar hydrodynamic and morphological changes in the aqueous humor outflow pathway after washout and Y27632 treatment in monkey eyes. *Exp Eye Res*. 2011;93:397–404.
15. Yang CY, Liu Y, Lu Z, Ren R, Gong H. Effects of Y27632 on aqueous humor outflow facility with changes in hydrodynamic pattern and morphology in human eyes. *Invest Ophthalmol Vis Sci*. 2013;54:5859–5870.
16. Gong H, Yang CY. Morphological and hydrodynamic correlations with increasing outflow facility by rho-kinase inhibitor Y-27632. *J Ocul Pharmacol Ther*. 2014;30:143–153.
17. Ren R, Li G, Le TD, Kopczynski C, Stamer WD, Gong H. Netarsudil increases outflow facility in human eyes through multiple mechanisms. *Invest Ophthalmol Vis Sci*. 2016;57: 6197–6209.
18. Overby D, Gong H, Qiu G, Freddo TF, Johnson M. The mechanism of increasing outflow facility during washout in the bovine eye. *Invest Ophthalmol Vis Sci*. 2002;43:3455–3464.
19. Braakman ST, Read AT, Chan DW, Ethier CR, Overby DR. Colocalization of outflow segmentation and pores along the inner wall of Schlemm's canal. *Exp Eye Res*. 2015;130:87–96.
20. Allingham RR, de Kater AW, Ethier CR, Anderson PJ, Hertzmark E, Epstein DL. The relationship between pore density and outflow facility in human eyes. *Invest Ophthalmol Vis Sci*. 1992;33:1661–1669.
21. Grierson I, Lee WR, Abraham S, Howes RC. Associations between the cells of the walls of Schlemm's canal. *Albrecht Von Graefes Arch Klin Exp Ophthalmol*. 1978;208:33–47.
22. Ye W, Gong H, Sit A, Johnson M, Freddo TF. Interendothelial junctions in normal human Schlemm's canal respond to changes in pressure. *Invest Ophthalmol Vis Sci*. 1997;38: 2460–2468.
23. Denk W, Horstmann H. Serial block-face scanning electron microscopy to reconstruct three-dimensional tissue nanostructure. *PLoS Biol*. 2004;2:e329.
24. Jungreuthmayer C, Steppert P, Sekot G, et al. The 3D pore structure and fluid dynamics simulation of macroporous monoliths: high permeability due to alternating channel width. *J Chromatogr A* 2015;1425:141–149.
25. Kreshuk A, Walecki R, Koethe U, et al. Automated tracing of myelinated axons and detection of the nodes of Ranvier in serial images of peripheral nerves. *J Microsc*. 2015;259:143–154.
26. Hammer S, Monavarfeshani A, Lemon T, Su J, Fox MA. Multiple retinal axons converge onto relay cells in the adult mouse thalamus. *Cell Rep*. 2015;12:1575–1583.
27. Kuwajima M, Spacek J, Harris KM. Beyond counts and shapes: studying pathology of dendritic spines in the context of the surrounding neuropil through serial section electron microscopy. *Neuroscience*. 2013;251:75–89.
28. Young RD, Knupp C, Pinali C, et al. Three-dimensional aspects of matrix assembly by cells in the developing cornea. *Proc Natl Acad Sci U S A*. 2014;111:687–692.
29. Mustafi D, Kikano S, Palczewski K. Serial block face-scanning electron microscopy: a method to study retinal degenerative phenotypes. *Curr Protoc Mouse Biol*. 2014;4:197–204.
30. Scott PA, Lu Z, Liu Y, Gong H. Relationships between increased aqueous outflow facility during washout with the changes in hydrodynamic pattern and morphology in bovine aqueous outflow pathways. *Exp Eye Res*. 2009;89:942–949.
31. Deerinck TJ, Bushong E, Thor A, Ellisman M. NCMIR methods for 3D EM: a new protocol for preparation of biological specimens for serial block face scanning electron microscopy. *Microscopy*. 2010;6–8.
32. Grierson I, Lee WR. Pressure-induced changes in the ultrastructure of the endothelium lining Schlemm's canal. *Am J Ophthalmol*. 1975;80:863–884.
33. Grierson I, Lee WR. Light microscopic quantitation of the endothelial vacuoles in Schlemm's canal. *Am J Ophthalmol*. 1977;84:234–246.
34. Tripathi R, Tripathi B. Functional anatomy of the anterior chamber of the angle. In: Duane TD, Jaeger EA, eds. *Biomedical Foundations of Ophthalmology*. Manhattan, NY: Harper & Row; 1982.
35. Ethier CR, Coloma FM, Sit AJ, Johnson M. Two pore types in the inner-wall endothelium of Schlemm's canal. *Invest Ophthalmol Vis Sci*. 1998;39:2041–2048.
36. Bill A, Svedbergh B. Scanning electron microscopic studies of the trabecular meshwork and the canal of Schlemm–an attempt to localize the main resistance to outflow of aqueous humor in man. *Acta Ophthalmol (Copenh)*. 1972;50:295–320.
37. Johnson M, Shapiro A, Ethier CR, Kamm RD. Modulation of outflow resistance by the pores of the inner wall endothelium. *Invest Ophthalmol Vis Sci*. 1992;33:1670–1675.
38. Acott TS, Kelley MJ. Extracellular matrix in the trabecular meshwork. *Exp Eye Res*. 2008;86:543–561.
39. Acott TS, Kelley MJ, Keller KE, et al. Intraocular pressure homeostasis: maintaining balance in a high-pressure environment. *J Ocul Pharmacol Ther*. 2014;30:94–101.
40. Lee J, Schmid-Schönbein GW. Biomechanics of skeletal muscle capillaries: hemodynamic resistance, endothelial distensibility, and pseudopod formation. *Ann Biomed Eng*. 1995;23: 226–246.
41. Raucher D, Sheetz MP. Characteristics of a membrane reservoir buffering membrane tension. *Biophys J*. 1999;77: 1992–2002.
42. Pedrigi RM, Simon D, Reed A, Stamer WD, Overby DR. A model of giant vacuole dynamics in human Schlemm's canal endothelial cells. *Exp Eye Res*. 2011;92:57–66.
43. Grierson I, Lee WR. Changes in the monkey outflow apparatus at graded levels of intraocular pressure: a qualitative analysis by light microscopy and scanning electron microscopy. *Exp Eye Res*. 1974;19:21–33.
44. Johnstone MA, Grant WG. Pressure-dependent changes in structures of the aqueous outflow system of human and monkey eyes. *Am J Ophthalmol*. 1973;75:365–383.
45. Brilakis HS, Johnson DH. Giant vacuole survival time and implications for aqueous humor outflow. *J Glaucoma*. 2001; 10:277–283.
46. Johnson M, Ethier CR. *Problems in Biomedical Fluid Mechanics and Transport Phenomena*. Cambridge: Cambridge University Press; 2013.
47. Grierson I, Lee WR. Pressure effects on flow channels in the lining endothelium of Schlemm's canal. A quantitative study by transmission electron microscopy. *Acta Ophthalmol (Copenh)*. 1978;56:935–952.
48. Bill A. Scanning electron microscopic studies of the canal of Schlemm. *Exp Eye Res*. 1970;10:214–218.
49. Lee WR, Grierson I. Pressure effects on the endothelium of the trabecular wall of Schlemm's canal: a study by scanning electron microscopy. *Albrecht Von Graefes Arch Klin Exp Ophthalmol*. 1975;196:255–265.
50. Cha ED, Xu J, Gong L, Gong H. Variations in active outflow along the trabecular outflow pathway. *Exp Eye Res*. 2016;146: 354–360.

Investigative Ophthalmology & Visual Science

51. de Kater AW, Melamed S, Epstein DL. Patterns of aqueous humor outflow in glaucomatous and nonglaucomatous human eyes. A tracer study using cationized ferritin. *Arch Ophthalmol*. 1989;107:572–576.
52. Chang JY, Folz SJ, Laryea SN, Overby DR. Multi-scale analysis of segmental outflow patterns in human trabecular meshwork with changing intraocular pressure. *J Ocul Pharmacol Ther*. 2014;30:213–223.
53. Braakman ST, Pedrigi RM, Read AT, et al. Biomechanical strain as a trigger for pore formation in Schlemm's canal endothelial cells. *Exp Eye Res*. 2014;127:224–235.

Investigative Ophthalmology & Visual Science